A HISTOLOGICAL AND IMMUNOLOGICAL RESPONSE STUDY OF AN IMPLANTABLE MICROCAPSULE DRUG DELIVERY DEVICE FOR THE TREATMENT OF GLIOBLASTOMA

by
Graham Van Schaik
Submitted to the Department of Materials Science and Engineering in
Partial Fulfillment of the Requirements for the Degree of
Bachelor of Science in Materials Science and Engineering at the
Massachusetts Institute of Technology
~~May 2012~~ [June 2012]

Signature redacted

Signature of Author ....

Graham W. W. Van Schaik
Dept. of Materials Science and Engineering
May, 2012

Signature redacted

Certified by..

Michael J. Cima
Sumitomo Electric Industries Professor of Engineering
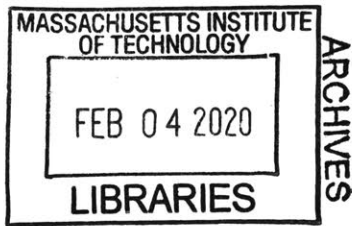Thesis Supervisor

Signature redacted

Accepted by ....

Chris Schuh
Department Head
Department of Materials Science and Engineering

A Histological and Immunological Response Study of an Implantable Microcapsule Drug Delivery Device for the Treatment of Glioblastoma.

by
Graham Van Schaik
Submitted to the Department of Materials Science and Engineering
in Partial Fulfillment of the Requirements for the Degree of
Bachelor of Science in Materials Science and Engineering
at the Massachusetts Institute of Technology

ABSTRACT

Glioblastoma Multiform (GBM) and the more prevalent metastatic brain tumor are some of the most deadly forms of cancer, accounting for the death of nearly 14,000 individuals yearly. Previous treatment options for brain cancers include tumor resection, radiation, and chemo therapy but such options provide limited success in prolonging patients' life. Most patients experience tumor recurrence near the resected areas within a few months and are ineligible for additional rounds of chemotherapy due to systemic toxicity associated with many chemotherapeutic drugs. Advances in implantable drug delivery devices look promising, but can suffer from the possibility of biofouling, or loss of function due to a patient's own immune response.

An implantable microcapsule device, designed to deliver locally chemotherapeutics in the brain, was developed by Alex Scott and Yoda Patta in the Cima Lab at the MIT Koch Institute for Integrative Cancer Research. The device passively delivers a payload of two common chemotherapeutics, Doxorubicin HCl or Temozolomide, and can be inserted post tumor resection to limit the possibility of tumor recurrence. In vivo implantation and sham surgeries using the device cap were performed on Sprague Sawley rats to assess an immune response and to look for potential biofouling 3, 7, 14, and 28 days post surgery. Immune response was quantified using a μBCA assay for total protein concentration and an ELISA targeting Glial Fibrillary Acidic Protein (GFAP). Histology assays targeting 3 markers for new cell growth GFAP, NeuN, and CD68, were performed to determine relative location and prevalence of potential biofouling.

Histological analysis offered little insight in the potential for biofouling near the implantation site as little fluorescence was seen for any markers. Fluorescence was slightly higher on the edge of the implantation wound site, but this may have been due to factors other than the increased presence of protein. ELISA and μBCA analysis suggested that the immune response was activated and biofouling a possibility as total protein concentration was significantly higher 3 days post surgery than that seen at later time points ($p < 0.05$) and GFAP concentration for implantation groups remained elevated throughout the study.

ACKNOWLEDGEMENTS

This work was completed with the constant support and guidance of many individuals, each of whom I would like to thank sincerely.

Professor Michael Cima for allowing me to be a part of his lab for the past 2 years; his teaching, guidance, and support as my professor and thesis adviser were truly invaluable.

Yoda Patta for her tireless efforts helping me to learn in the classroom and in the lab. Without her constant assistance and above all else, constant friendship, this work would not have been possible—I am truly better for having had the opportunity to work with her.

Jay Cy for his patience and research expertise, especially for his assistance performing implantation surgeries and guidance during my protein and histology assays. Also, the rest of the Cima lab who have all helped me at one time or another: Byron, Kevin, Lenny, Maple, Qunya, Vincent, and Syed.

Finally, my family. In particular my mother, father, and sister, Katherine, who were always willing and eager listeners, providing congratulations when things worked and support when they did not.

TABLE OF CONTENTS

LIST OF TABLES AND FIGURES

1 BACKGROUND AND MOTIVATION

1.1 Glioblastoma Multiforme and Metastatic Brain Cancer

Glioblastoma Multiforme is "the most malignant glial tumor and one of the most deadly forms of cancer [8]." The annual occurrence of malignant primary brain tumors is 5-8 cases/100,000 individuals [1]. Glioblastoma Multiforme (GBM), an infiltrative and vascularized astrocytoma, is responsible for a majority of such tumors and is quite nearly a death sentence for those diagnosed. Composed of necrotic cells and numerous cancer cell types, each in different stages of development, GBM is very difficult to eradicate and prognosis is quite poor. Median survival among patients receiving the maximum treatment is between 12 to 18 months [18, 30] and in the interim, patients diagnosed with GBM experience a variety of maladies. Glial tumors can disrupt various brain functions resulting in patients with GBM tumors experiencing headaches, nausea, impairment of speech, hearing, vision, or balance, and even emotional changes and seizures.

Treatments for the disease are aggressive and limited. Typical treatment procedures often begin with a surgical resection of the tumor, in combinations with radiation treatment and chemotherapy [29, 30]. Due to high level of infiltration of GBM tumors, it is often impossible to completely resect the cell mass. Many patients undergoing resection thus often experience new GBM lesions within 2-3 cm of the resection margin [11, 12]. Figure 1 exhibits such a reoccurrence and underscores how challenging glioblastoma is to eradicate [11, 14].
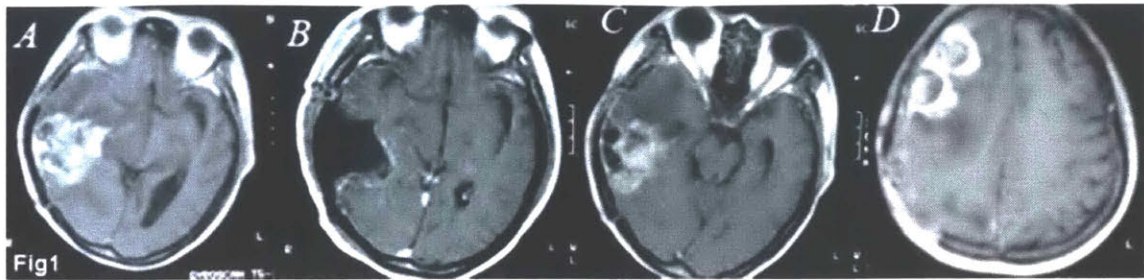
Figure 1. MRI of a 52 year old patient diagnosed with a malignant glioblastoma
View of the initial glioma (frame A). Tumor site post resection surgery (frame B). MRI images of a new growth in the original location 6 months later (frame C). Additional lesions distal to the first tumor in the ipsilateral formal lobe (frame D).

Taken from the MRI of a 52 year old patient diagnosed with a malignant glioblastoma, frame A provides a view of the initial glioma. The tumor, containing anaplastic ependymoma and astrocytoma (WHO grade III), was located in the right temporal lobe. Post resection (frame B), the patient was treated with one dose of radiation and three doses of chemotherapy. MRI's 6 months later revealed a new growth (WHO grade IV) in the original location (frame C) and additional lesions distal to the first tumor in the ipsilateral frontal lobe (frame D) [11].

Metastatic tumors in the brain are more common than GBM and account for nearly 24-45% of all cancer patients, causing 20% of all cancer deaths annually [13, 28]. Like GBM, metastatic cancers present with similar symptoms to glioblastoma and leave patients with a variety of sensory and motor dysfunction. Metastatic tumors in the brain pose additional challenges to physicians because of their ability to form multiple tumors in a variety of locations within the brain. Unsurprisingly, prognosis for such lesions is generally quite poor, especially since a majority of patients with metastatic tumors are often diagnosed in the late stages of tumor growth. This small window for treatment limits what can be done to combat tumor growth and any treatments available are dependent on the type of cancer, as well as the location of the tumors [9, 13, 17]. Resection of multiple tumors is rarely performed because of the risks associated with such surgeries. Typical treatment regimes involve a combination of radiation

7

therapy and chemotherapy and are designed to treat system-wide due to the dispersive

characteristic of metastatic cancers [13, 17]. A downside of these treatments is that they may be

limited in their dosage and scope due to previous cancer treatments. Another consequence of

metastatic tumors in the brain is that in order to ensure a sufficient concentration of

chemotherapeutic cancer drug reaches the brain through the blood brain barrier (BBB), any non

local delivery must be given in very high dosages [30].

1.2 The Blood Brain Barrier

Brain capillary

Endothelial cell

Water, oxygen, and glucose

Astrocyte

Neuron

Cerebrospinal fluid

Blood flow
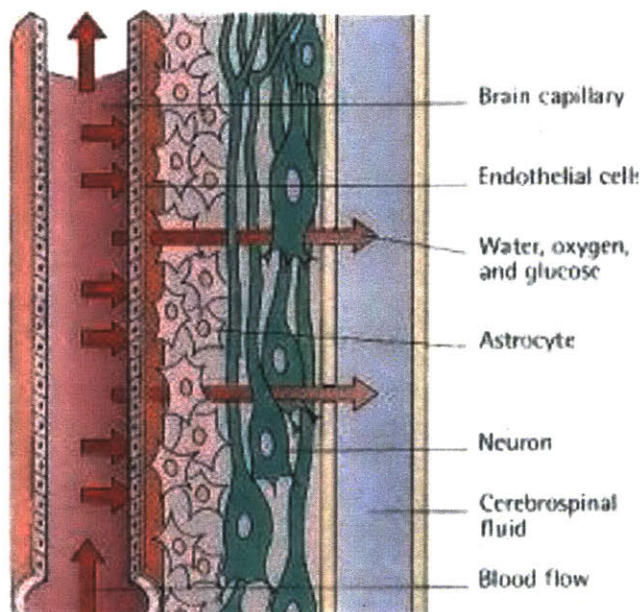
Figure 2. Schematic of the Blood Brain Barrier transverse to a capillary [31]

Complicating the treatment of GBM and metastatic tumors in the brain, the blood brain

barrier prevents the passage of many chemotherapeutic drugs from reaching their target. The

basic construction of the blood brain barrier (figure 2) is supported by tightly joined endothelial

cells. The tight intercellular junctions of these cells enable the selective passage of certain

molecules into the brain while preventing others. Properties of this barrier can vary with time

depending on the external surroundings of the brain [8], and generally, small, hydrophobic or

8

lipophilic molecules, like oxygen, glucose, or hormones stand the best chance of passing through the BBB. After making it from the blood stream through the endothelial cells, a molecule must continue to pass through layers of astrocytic cells and neurons before reaching the cerebrospinal fluid (CSF) [10]. The CSF which is primarily composed of water, is responsible for promoting the passage of necessary molecules into the brain itself and drugs passing through the BBB are exchanged into the brain from the CSF. Given this method of exchange, it is crucial to ensure that any intravenously injected chemotherapeutic drugs are capable of exchanging with the brain.

1.3 Common Chemotherapeutic Drugs for GBM and Their Limitations

Two drugs, Temozolomide (TMZ) and Doxorubicin Hydrochloride (DOX), have proven effective in treating numerous forms of cancer, including GBM, and have been studied extensively since their inception in the 1980's and 1950's [30]. A prodrug, Temozolomide is biologically hydrolyzed at and above neutral pH to form a compound (known as MTIC) which forms a cytotoxic molecule by the time it reaches the tumor site [4]. MTIC causes methylation of tumor cell DNA and subsequent breaks in the single and double stranded helix. These breaks are responsible for eventual apoptotic cell death. Despite an estimated TMZ bioavailability of 100% [21], the active drug MTIC has a short half life of 2 minutes and TMZ was shown to be rapidly absorbed and subsequently eliminated by the body [21].

Doxorubicin Hydrochloride is composed of a planar anthracycline ring. This structure enables the drug to both intercalate into the DNA helix of tumor cells and disrupt the progression of certain DNA enzymes. The net result is a tumor cell which is unable to synthesize new DNA and will eventually die [30]. DOX has a low bioavailability due to its large molecular weight and low lipophilicity and therefore is rarely used for the type of systemic brain delivery required

to treat GBM or metastatic tumors in the brain. The low degree to which Doxorubicin passes through the blood brain barrier is underscored by the results of a study carried out by Voulgaris et al. which reported that a direct injection of DOX into tumor sites yielded a concentration 25 times higher than that from intravenous delivery. These setbacks with DOX are compounded by the fact that DOX can lead to cardiotoxicity if a lifetime total of 450-550 mg/m^2 is exceeded [7]. To improve the efficacy of treatment with DOX, modifications to the original chemical structure have been made. One modification in particular, a liposomal form of the drug marketed under the name Doxil®, has shown to improve greatly the availability of DOX at tumor sites [7, 32].

The development of prodrug forms and liposomal variants of chemotherapeutic drugs has increased the amount of active drug capable of reaching the tumor site, but there are still limitations associated with systemic delivery. Previous studies on TMZ have shown that dosages below toxic levels over a 21 day period have led to signs of lymphopenia [24, 32]. This leaves researchers and physicians striving for a means of drug delivery which would enable them to overcome the negative effects of high-dosage systemic delivery, while still realizing the benefits of high drug concentrations near the tumor site.

1.4 Medical Drug Delivery Devices and Associated Challenges

Recently treatment methods have moved into the field of targeted drug delivery devices that act as a passive, diffusion-based means of getting chemotherapeutic drugs directly to a tumor site. Passive delivery mechanisms come in multiple forms ranging from biodegradable polymers impregnated with chemotherapeutic drugs to biocompatible reservoirs containing a drug payload. Both cases rely on the drug diffusing out from the device (either through an orifice or through device degradation) and into the surrounding cancer tissue. Each type of

device is characterized by a different diffusion profile with the former yielding an initial spike in drug concentration followed by a linear release rate and the latter, diffusion based on Fick's First Law [16]. Researchers have successfully experimented with different copolymer formulations in an effort to tune the time to release from these devices [21].

Some implantable depots, like Gliadel®, have found limited success. Gliadel® wafers are made from Carbophenoxypropane:sebacic acid copolymer systems (CPP:SA) and a chemotherapeutic agent Carmustine (BCNU). These wafers are implanted in and around tumor sites and carry a payload of approximately 7.7 mg of BCNU. Gliadel® usage two to three weeks after tumor resection showed an increase in patient survival rate from 6% to 31% after 2 years [5], though these devices are not without drawbacks. Most noticeably the short distance over which they are effective (approximately 3mm or less) as well as numerous other health effects ranging from edema at the implantation site to CSF leakage, hydrocephalus, and seizures [5, 10].

Aside from Gliadel®, a small microcapsule drug delivery device made of Vectra MT 1300 liquid crystal polymer (LCP) was developed by Alex Scott and Yoda Patta of the Cima Lab at MIT. Devices were designed for treatment of brain tumors with both TMZ and DOX.
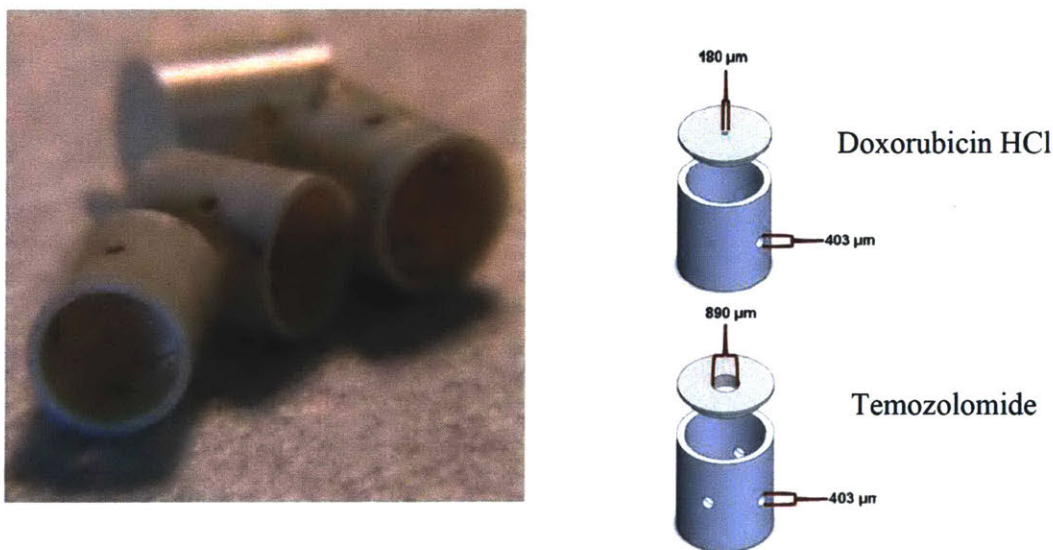
Figure 3. Schematic of LCP microcapsule devices. Cap bore hole for diffusion differs with respect to the type of drug being delivered. For delivery of Doxorubicin HCL (top) diameter = 180 μm and Temozolomide (bottom) 890 μm [22].

Devices were tailored for either TMZ or Dox release by modification of the cap opening diameter (figure 3). Devices for DOX had a diameter of 180 μm on the top while TMZ devices had a diameter of 890 μm. Side orifices could be sealed using Dymax 1161-M UV-cured epoxy to further modify devices and tune the diffusion rate [16]. Overall, devices containing each drug with all holes open or no holes open exhibited diffusion according to Fick's first law with an initial linear rate [22].

One of the primary challenges associated with the inclusion of devices into the human body is the immunological response associated with it [15]. Just as the body reacts negatively to disease causing agents, all implantation surgeries elicit wound healing responses which may completely encapsulate the device in new tissue, blocking orifices and limiting treatment. Biofouling such as this is a limiting factor in many forms of drug delivery and often necessitates separate testing to ensure immune compatibility.

1.5 Wound Healing

1.5.1 Human immune response and the CNS

The human biological response can be divided into a series of stages beginning with the acute inflammation and ending with the formation of granulomatous tissue [2, 3, 20]. Initial wound response is followed by the body beginning to clean the affected site by increasing blood flow to the area and eventually forming a clot to prevent further contamination. Next, the "permeation of salts, proteins, and water through the endothelial tight junctions of capillary walls is increased, resulting in edema [23]." Additionally, this stage is characterized by the inflow of blood and tissue proteins to the affected area. Chronic inflammation follows the acute stage and the presence of larger macromolecules such as macrophages and lymphocytes can be detected.

Connective tissue begins to develop and the wound starts to restructure during this chronic phase. Lastly, the clot formed during the acute inflammatory phase is converted into granulation tissue and the foreign particle is surrounded by a layer of what eventually becomes an extracellular matrix sealing off the object from the rest of the body [27, 33].

The response of the human brain and the central nervous system, however, is altered.
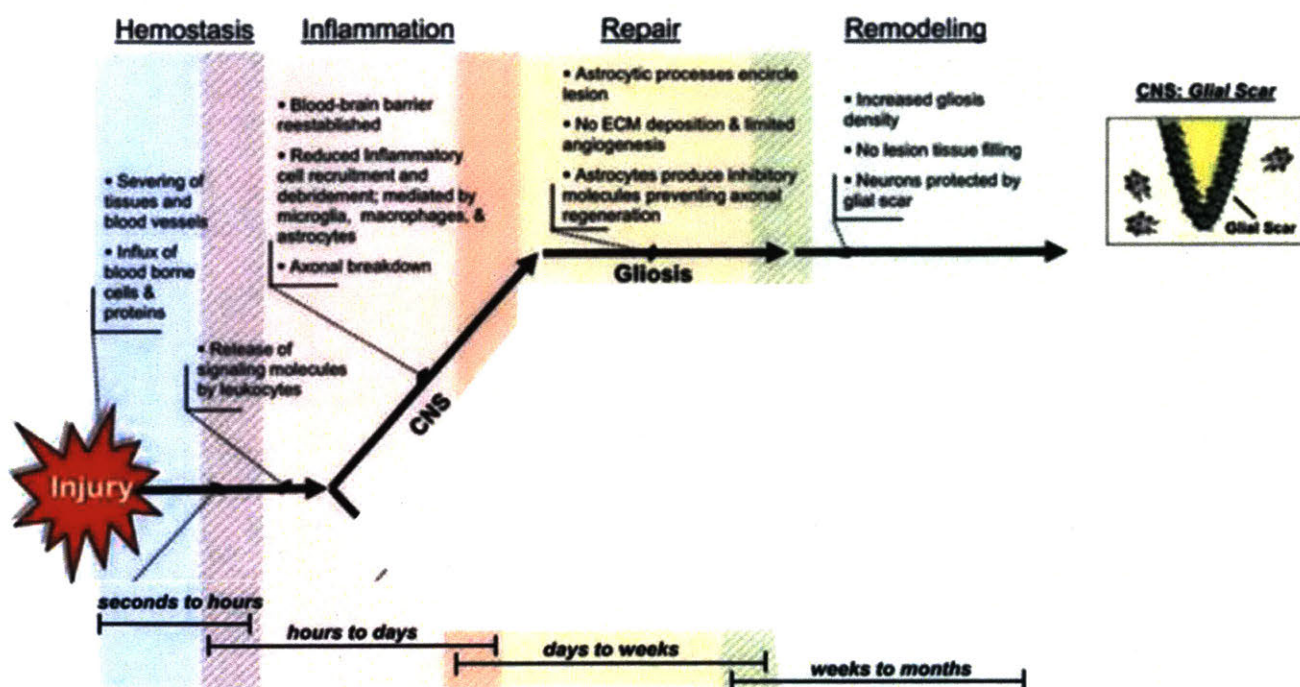
Figure 4. Schematic of the stages of an immune response mounted in the Central Nervous System (CNS).

Generally, wound healing in the human brain requires a larger amount of time than elsewhere due to the restrictiveness of the BBB in allowing the passage of large macromolecules. The combination of a restructured BBB and release of anti-inflammatory signaling factors results in decreased swelling in the brain. Therefore, a majority of wound healing in the CNS is carried out by secondary effector cells – astrocytes – near the injured brain tissue (Figure 4). These astrocytes are responsible for a variety of roles during the wound healing process including, the

provision of growth factors and mechanical support for neurons, the creation and maintenance of the blood–brain barrier, and the control of surrounding chemical environment through neurotransmitters and ion regulation [23].

1.5.2 CNS Healing Proteins

A number of markers are used to measure relative wound severity and healing rate during brain recovery. These markers can take the form of proteins or new neuronal cell formation and are visualized via staining with monoclonal antibodies. This work in particular will utilize three different markers, more specifically:

1) **Glial Fibrillary Acidic Protein (GFAP)** – a protein expressed by astrocytes for a variety of purposes, including the functioning of the BBB and cell signaling, though its role in the formation of Glial scars will be most pertinent to this research. GFAP is visualized using anti GFAP antibodies.

2) **Young Neuronal Cells** – The presence of young neuronal cells indicates that wound healing has begun. These young cells express certain cell markers which are able to be recognized by NeuN, a neuronal nuclear antigen.

3) **Integrin beta-3 (β3) or CD68**—a cell marker expressed by activated rat microglia, visualized with an anti-ED1/CD68 antibody.

1.6 Modeling and Measuring Wound Healing

A number of in vitro and in vivo assays may be used to measure wound healing in the brain. These assays are crucial to understanding how the incorporation of specific medical devices will affect brain function as well as healing. A common in vitro model which has been employed to determine healing is the "scratch" test, or cell migration assay. This assay involves

disrupting or "scratching" the surface of a cellular monolayer and observing how the distressed cells migrate across the disturbance (heal) over a timeframe [31]. This method enables researchers to visualize the very beginnings of wound healing in real-time, as most experiments are performed in the presence of photographic equipment.

In vivo models for human brain response are typically carried out using an animal model similar to humans. It is common for Sprague-Dawley rats to be chosen for such assays because their physical response to brain injuries are accelerated and yields similar symptoms to those in humans. Despite having different underlying causes, results obtained regarding fibrous encapsulation in the rat brain model are usable [6]. Additionally, rats are far more beneficial than other animal models due to their relatively low living requirements (food, shelter, etc.) and their docile behavior [6]. Typical assays involve implantation of a biomedical device into the rat brain via surgical means, and subsequent sacrificing of rats at given time points to observe the effects of such trauma on healing. This work will utilize the Sprague-Dawley model outlined above for the reasons suggested here. Animals will undergo surgery with implantation of the DOX cap of the LCP microcapsule drug delivery device and brains will be harvested at 3, 7, 14, and 28 days post surgery to ascertain concentrations of various markers of immune resposne. Once harvested, rain brains can be treated with a variety of protocols to yield particular results depending on the goals of the research.

Generally the brains undergo some form of homogenization to extract desired components. The homogenate is then subjected to any number of assays. Analytical techniques include: micro bicinchoninic acid (BCA) tests for total protein concentration, sodium dodecyl sulfate polyacrylamide gel electrophoresis (SDS-PAGE) for separating proteins, Western Blots to determine the purity and molecular weights of proteins within a sample, or Enzyme-Linked

Immunosorbent assays (ELISA) which detect and quantify the presence of a certain antibody molecular marker [25]. Additionally, radio-immunoprecipitation (RIP) assays could be used to determine the rate of protein generation. Each of these assays has strengths and weaknesses based on time and availability of resources. This particular study will make us of a μBCA assay to quantify initial protein concentration for successful dilution, and then an ELISA analysis to quantify the amount of GFAP. This assay was chosen in lieu of any other because of its relative ease and high sensitivity. Additionally, previous research indicates that the protein in question, GFAP, will be present and it is therefore not necessary to identify it before it is quantified.

Another commonly used, less quantitative assay, for wound healing is immunohistology. Designed to visualize particular tissue types and proteins within a tissue sample, immunohistology is an effective means of determining presence, location, and abundance or certain markers of healing. Generally performed on slices of tissue ranging from 5 to 20 μm in thickness, samples can be fixed using a variety of methods from plasticizers to cryogenic freezing. Once sliced, the tissue slides can be stained with primary antibodies conjugated to a label and then marker location visualized. Due to restrictions set forth by the Koch Institute Histology Core, this research will use cryogenically frozen brains from healing rats, sectioned into slices approximately 6-8μm in thickness. These slices will be dyed with immunofluorescent markers anti GFAP, CD-68, and NeuN and visualized.

1.7 Thesis Objectives

This work seeks to utilize a Sprague-Dawley rat model to understand better how the wound healing response affects the success of a newly designed biomedical device. More specifically, the study will make use of various analytical techniques to identify and quantify specific markers of the wound healing process which are responsible for potential biofouling. The second goal is to

visualize the location and abundance of new cell growth in an effort to determine better the proper placement and orientation of LCP devices to maximize effectiveness of the device. As stated previously, many cancers require a highly targeted, highly specific transfer of drug payload to maximize treatment efficiency, it is crucial that the device not be hampered by the wound healing process.

2 MATERIALS AND METHODS

2.1 Device Implantation and Sham procedure

To assess wound healing, a rat model was used in this work. The cap of a single LCP DOX microcapsule device (designed by Alex Scott at MIT) was implanted in the intracranial space of a 200-250g female Sprague-Dawley rat obtained from Charles River. All surgery and post-operation care was conducted in accordance with the federal guidelines and MIT Committee on Animal Care policies. Rats received a subcutaneous shot of Burprenorphine (0.5 mg/kg) prior to surgery and every 8-12 hours post surgery for 48 hours. Anesthetization occurred with continuous flow of isoflurane gas (O_2 with 2-2.5% isoflurane). The rats' anesthesia was monitored via dorsal foot reflex and maintained throughout the course of the surgery. When fully anesthetized, rats were prepared for surgery by shaving their heads and disinfecting the area with an alternating sequence of betadine scrubs followed by alcohol (3x).

All intracranial surgeries were performed under a stereoscope. An initial midline incision was made (approx 2 cm). This was followed by the opening of the rat's membrane around where the burr hole would be. A motorized dental drill with a 0.9 mm diameter Aseptico tip was used to make an opening in the skull. A slight indentation was made in the left cortex, approximately 2 mm from the midline suture and 1-2 mm from the lambda. Special care was taken to avoid the

midline sutures and to not drill through the dura, minimizing excess bleeding. To expose the brain where the device cap was to be inserted, jeweler's scissors and forceps were used to cut the dura, and the cap was inserted parallel to the midline. Once the device was inserted such that it was no longer visible, the incisions were closed using sutures and tissue glue, and rats were monitored for morbidity. For rats used in the sham treatment, the device was inserted as described previously, but removed after 10 minutes. Burprenorphine (0.05 mg/kg) was administered to all rats undergoing surgery at 8-12 hour intervals for 48 hours to alleviate pain.
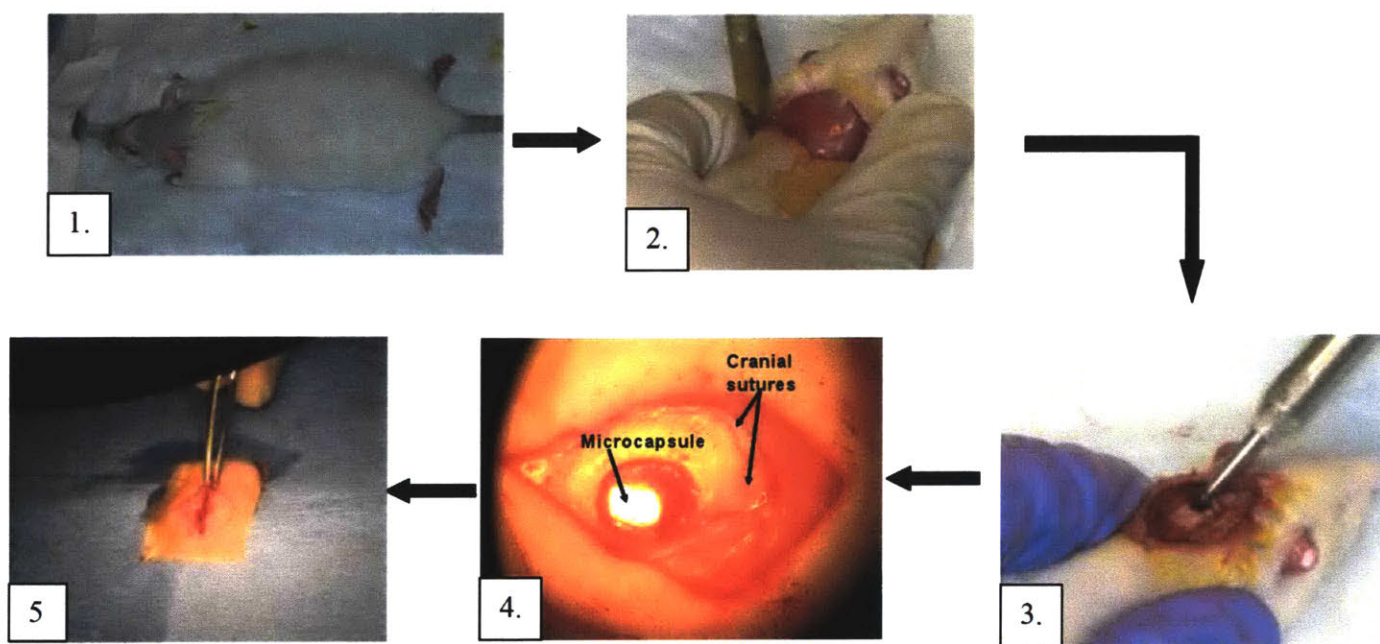
Figure 5. Schematic of Implantation/Sham surgeries.
All steps for implantation and sham surgeries were equivalent aside from actual implantation. Rats were anesthetized with isoflurane, shaved for surgery, and cleaned with alternating betadine, isopropyl alcohol scrubs (1). Initial incisions were made along the midline (2) and the skull drilled through (3). The device was implanted permanently or inserted for 10 minutes (4) and the wound sutured (5).

Rats from the implantation group and the sham group were sacrificed at 3, 7, 14, and 28 days post surgery and their brains were resected for protein analysis assays. All resected brains were frozen at -80°C within 30 minutes of resection to preserve proteins.

2.2 Homogenization for Protein Analysis Assays

Brains which were analyzed for GFAP concentration were homogenized to extract all protein from the tissue. All homogenization reagents and materials were prepared prior to thawing the brain tissue. Tissue homogenizer solution (FNN 0081, Invitrogen) was thawed from -20°C in a bath of cool water. The reagent was removed from the water when only a small amount of ice remained. While the reagent was thawing, amber eppendorf tubes (1.5 or 2 mL) were filled with 1 gram of ZrO beads in preparation for homogenization. Once the reagent was completely thawed, 0.25 mL of tissue homogenizer solution was added to each eppendorf and the tubes were closed and labeled. Brain tissue to be homogenized was removed from -80°C storage, the cerebellum was discarded and, if a non-sham rat, the device was removed from the frozen brain tissue. The brain was then immediately sliced starting from the posterior into 0.1 ± 0.02 g, sections which were placed into the eppendorf tubes with beads and homogenizer solutions. Sections of brain impinged upon by the device were noted.
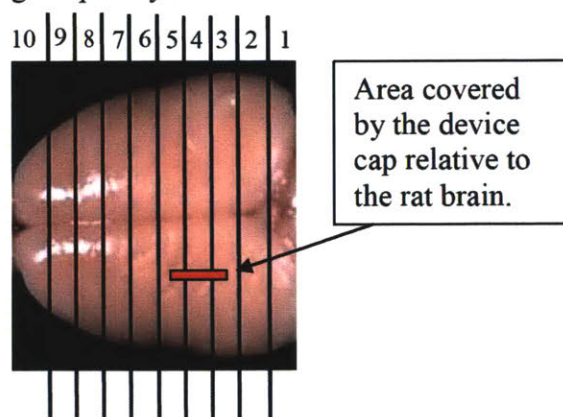
Figure 6. Serial 0.1g sections of brain tissue for total protein and GFAP analysis.

The tissue/homogenizer mixture was placed into a NextAdvance air-cooled tissue bead homogenizer to disrupt the tissue, and the homogenized solution was centrifuged for 10 minutes at 13.2 krpm and 4°C. The supernatant from each slice was transferred into a new centrifuge tube (one for each section) and centrifuged for 10 minutes under the same conditions. The new supernatant from each section was collected in a labeled eppendorf tube, and frozen at -20°C until needed.
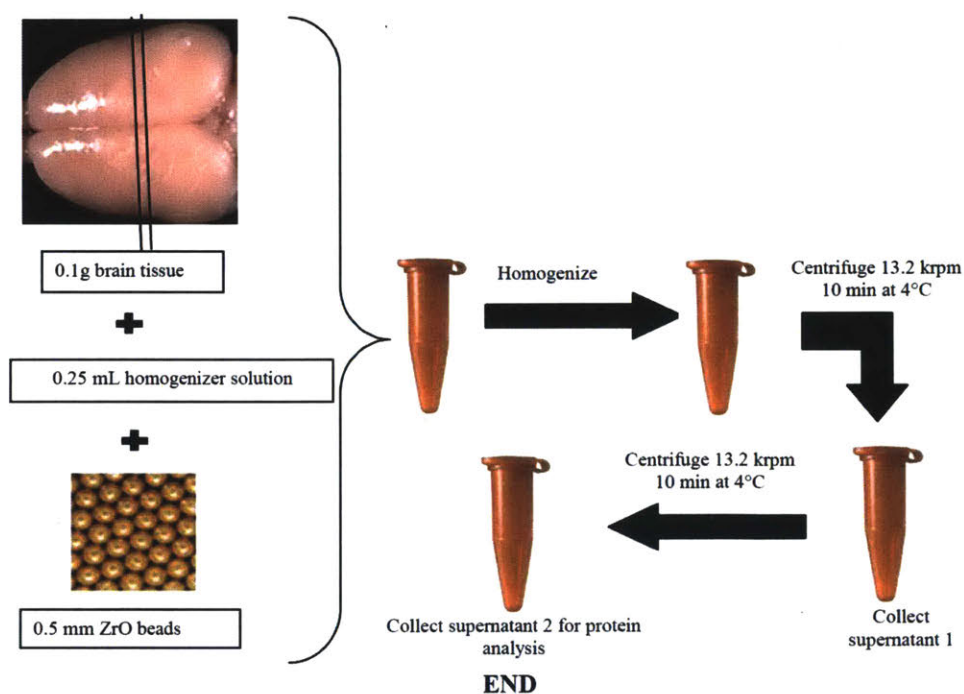
Figure 7. Brain Homogenization Method

2.3 Protein Assays

2.3.1 Micro Bicinchoninic Acid (μBCA) Protocol for Total Protein Concentration

Supernatant from the homogenization for each brain were thawed from -20°C and 200 μL from the samples of each brain which contained the LCP cap (typically 3 sections) were pooled

and gently mixed. 100 uL aliquots were taken from the pooled samples and serially diluted to a 1:1000 concentration in 1X PBS for the μBCA assay. All μBCA standards were prepared according to manufacturer's standards (ThermoScientific Pierce μBCA kit). Final concentrations of standards for comparison on the plates were: 50, 25, 12.5, 6.25, 3.125, 1.56 and 0.78 μg/mL. Once the μBCA working reagent was prepared from 24:25:1 parts Reagent A (MA), Reagent B (MB), and Reagent C (MC), 150μL of each standard and sample were pipetted into a 96 well plate. Duplicates were plated for each standard and triplicates for each sample. Next 150μL of the working reagent were pipetted into each well, the microplate was gently shaken for 30 seconds, and placed (covered) into an incubator at 37°C for 2 hours. Once taken out, the plate was cooled to room temperature and absorbance at 562 nm read.

2.3.2 Enzyme-Linked Immunosorbent Assay for GFAP Protein Concentration

Based on results obtained from μBCA, original pooled samples from homogenization were thawed and diluted 1:12,000 in 1X PBS. All reagents were prepared according to Millipore's standards. This included dilution of 10X wash buffer to 1X in deionized water and preparation of standards in concentrations of 100, 50, 25, 12.5, 6.25, 3.125, 1.56, and 0 ng/mL of GFAP. Once all reagents were prepared, the ANTI GFAP Coated Plate was washed by adding 300 μL of 1X Wash Buffer to each well and allowing the plate to incubate at room temperature for 5 minutes before the wash was discarded. Following the initial wash, 100 μL of each standard and quality control samples were pipetted into 2 wells and 100μL of each sample were pipetted into 3 wells. The plate was covered and incubated for 2 hours at room temperature on a plate shaker before being held in a refrigerator 4°C overnight. After refrigeration, the standards and samples were discarded, the plate was washed 4 times with 275 μL of 1X Wash Buffer per well (1 minute between washes) and 100μL of Anti-GFAP Detection Antibody was pipetted into

21

each well. The plate was re-covered and incubated at room temperature on a plate shaker for 1 hour.

Antibodies were discarded following incubation and the plate was washed again 4 times following the same protocol described above. Following the fourth wash, 100 μL of Enzyme Solution was pipetted into each well; the plate was covered, and incubated at room temperature on a plate shaker for 30 minutes. The Enzyme Solution was then discarded, the plate washed 6 more times according to the method outlined above, and 100 μL of TMB solution was added to each well. The plate was kept on an orbital shaker and color change was monitored visually. When the 100 ng/mL standard exhibited a dark blue color (approximately 20 minutes), the plate was removed and 100 μL of Stop Solution was added to each well. The plate was immediately placed on a plate reader and absorbance was measured at 450 nm.

2.4 Immunofluorescence (IF) Staining

2.4.1 Sectioning

Immediately post resection, rat brains to be used for histological analysis were embedded in cryomolds containing OCT compound and snap frozen with isopentane pre-cooled in liquid nitrogen. These blocks were stored at -80°C until ready for sectioning. When sectioned, the first 200 μm of brain and OCT were discarded and six- 6 μm sections were taken. Following these slices, another 200 μm of tissue was discarded and six more 6 μm slices were taken. This sectioning procedure was repeated twice more for a total of four times, yielding 24 slices per brain. Slices were mounted on superfrost plus slides (2 slices/slide) and stored at -80°C until staining.

22

2.4.2 Staining

Slides were taken from the -80°C freezer and allowed to thaw for 30 minutes in room temperature. Slices were then fixed in ice cold acetone for 5 minutes and allowed to air dry for 30 minutes. Samples were washed in Phosphate Buffer Solution (PBS)-Tween 20 for 2x2 minutes. The sections were incubated for 30 minutes with a 3% Bovine Serum Albumin (BSA) / 1X PBS solution to block any non-specific binding of immunoglobulin. Post serum blocking, Alexa Fluor® 488 conjugated mouse anti-Glial Fibrillary Acidic Protein (GFAP) diluted 1:1000 in 3%BSA/PBS (Millipore #MAB3402X) and mouse anti-rat monocytes/macrophages [CD68] monoclonal antibody diluted 1:250 in 3%BSA/PBS (Millipore #MAB1435) were added to sections on the left of the slides. To the serial sections on the right, NeuN polyclonal antibody diluted 1:1000 in 3%BSA/PBS was added (Millipore #ABN78) and the slides incubated with the primary antibodies overnight at 4°C.
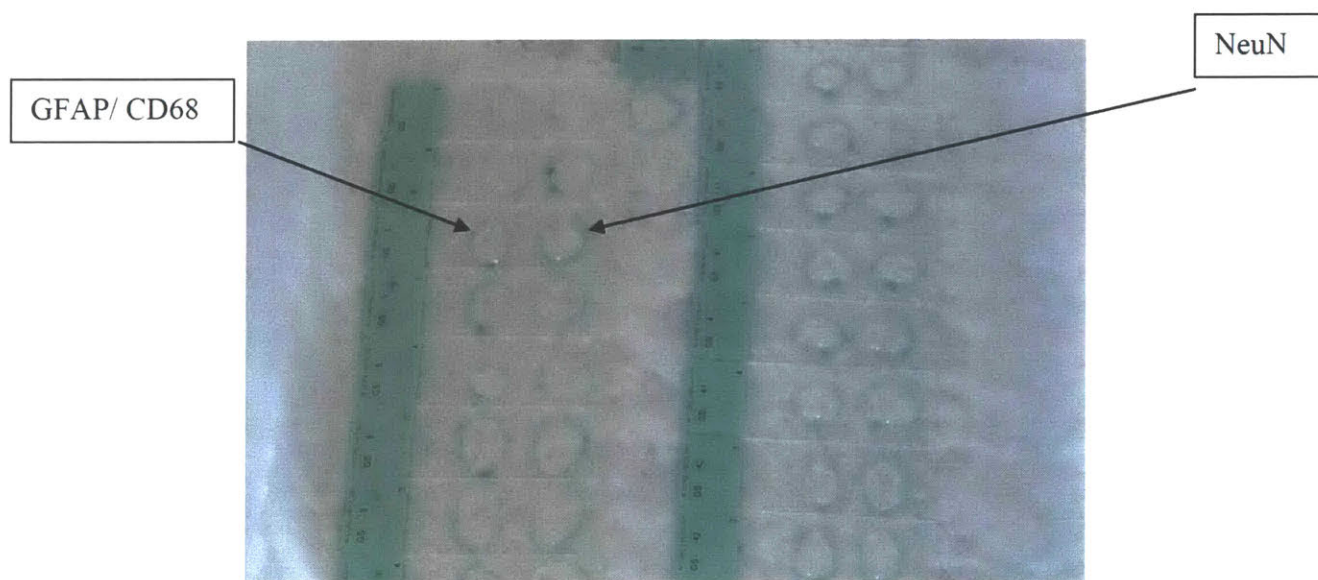
Figure 8. Samples for Immunofluorescence Histological Analysis.
Incubation with primary antibodies, GFAP and CD68 (left) and NeuN (right).

After 24 hours at 4°C, primary antibody solutions were decanted and slides were rinsed in PBS-Tween 20. From this point on, all slides were protected from light. Slices were incubated for approximately 3 hours at room temperature with Alexa Flour tagged secondary antibodies—Alexa Fluor 555 goat anti-mouse IgG (Life sciences, #'s A21422) for CD68 and Alexa Fluor 555 goat anti-rabbit IgG (Life Sciences #A21428) for NeuN, both diluted 1:2500 in 3%BSA/ PBS solution. Post incubation, slides were decanted, rinsed 3x2 minutes in PBS-Tween 20 and counterstained with 4,6-DIAMIDINO-2-PHENYLIN (DAPI 1:50,000) obtained from Life Sciences (#D1306). A final rinse was performed using PBS- Tween 20 and the slides were rinsed in DI water to prepare them for coverslipping.

One to two drops of Fluor-Gel (Electron Microscopy) were placed onto each side of the slide and spread carefully over the surface. Anti-fade coverslips were placed over the gel, air bubbles eliminated, and samples stored at in the dark at 4°C until visualization.

2.4.3 IF Visualization

Visualization was performed on an AMG Evos fl ALL-IN-ONE, digital inverted fluorescence microscope. Slides were continuously shielded from direct light for the duration of the whole visualization phase. Once in the microscope, the wound site was located on each slice and imaged for GFP, RFP, and DAPI. The contralateral portion of each brain slice was also imaged for those samples which exhibited noticeable fluorescence of GFAP, NeuN, or CD 68 at the wound site.

3 RESULTS

This thesis project sought to understand better how the wound healing response affects the success of a biomedical device. Using rat brains as an animal model for human CNS

immune response, specific markers of the wound healing process thought to be responsible for potential biofouling were identified and quantified. The location and abundance of new cell growth was visualized in an effort to determine better the proper placement and orientation of LCP devices to maximize the effectiveness of the device.

3.1 Empirical Rat Observation

To help eliminate any confounding variables associated with side effects to surgery, anesthesia, or pain management, rodents were visually monitored for morbidity or decreased neural function throughout the duration of the experiment. Over the 4 week study, no mortality was recorded and all rats undergoing surgery (sham or implantation) appeared to be functioning normally. No noticeable differences in appetite were recorded and external wound healing of the dermis progressed nicely. Rat motor function appeared unhampered post pain management and typical rodent behaviors of feeding and rest were observed.

3.2 μBCA Assay for Total Protein Concentration

Assays for total protein concentration were performed in an effort to determine the change of protein concentration over the course of the 4 week study. μBCA analyses were carried out iteratively on each brain sample in triplicates at various dilutions. This was done to ensure the model accurately predicted the total protein levels from the three 0.1 g sections of brain tissue impinged upon by the LCP cap during surgery. The standard curve derived from the μBCA assay had an R^2 value > 99% suggesting an accurate means of quantifying total protein concentration. Assays were carried out for rats which underwent implantation surgery as well as sham surgery and these results (adjusted against blanks) were used to determine the final

concentration of GFAP within each rat brain, analyzed as a function of the total protein concentration in the brain.

Table 1. Average µg/mL Total Protein isolated in three-0.1g slices of rat brain 3,7,14, and 28 days post surgery

|	Implanted (µg/mL)	Sham (µg/mL)
3 Days	55,640	65,141
7 Days	47,348	43,141
14 Days	39,253	41,566
28 Days	40,556	49,343

Note: Final dilution of protein samples used for this analysis was 1:1000 and this dilution factor was corrected for in the above table. Brains were harvested at 3, 7, 14, and 28 days after surgery with "Implanted" referring to surgery in which devices remained in the animal and "Sham" those which the devices were inserted and removed. Data obtained for implanted devices were averaged from a sample size n=4 rodents per duration while n-sham=1.

The data presented in Table 1 show that total protein concentration in the brain was elevated 3 days after surgery to 55,640 and 65,141 µg/mL for implanted and sham rats. Three days post surgery, the CNS was still undergoing the primary immune response of limited inflammation and elevated protein levels in the brain within that time period are reasonable. These levels decline by the end of 28 days, returning to perceived baselines of 40,556 and 49,343 µg/mL. It should be noted that total protein at the 28 day mark for both sham and implant rats increased from the previous time point, though were still less than the value at the 3 day mark.

A one-way Analysis of Variance Analysis (ANVOVA) (α=0.5, n=4) performed on implanted data yielded p=0.002 < 0.05, revealing a statistically significant difference in total protein concentration among implanted treatment levels. The results of this ANOVA are summarized in table 2.

Table 2. Analysis of Variance for Total Protein- Implantation Surgery, using Adjusted SS for Test						
Source of Variation	**SS**	**df**	**MS**	**F**	**P-value**	**F crit**
Between	$5.73*10^8$	3	$1.91*10^8$	10.44	0.002	3.59
Within	$2.01*10^8$	11	18294327	-----	-----	-----
Total	$7.74E*10^8$	14	-----	-----	-----	-----
S = 4277.19 R-Sq = 74.00% R-Sq(adj) = 66.91% α=0.05, n=4* *outliers were removed from 3 Days, yielding n=3						

To determine where the significant difference lay, a Tukey Post-Hoc test ($\alpha=0.05$) was performed on relevant data. Results showed that the concentration of total protein at 3 days was significantly greater than at 14 days (p=0.002), and 28 days (p=0.004) in implanted samples. These results of the Tukey-Post Hoc are shown explicitly in table 5 in appendix A. The trends are summarized graphically in figure 9.
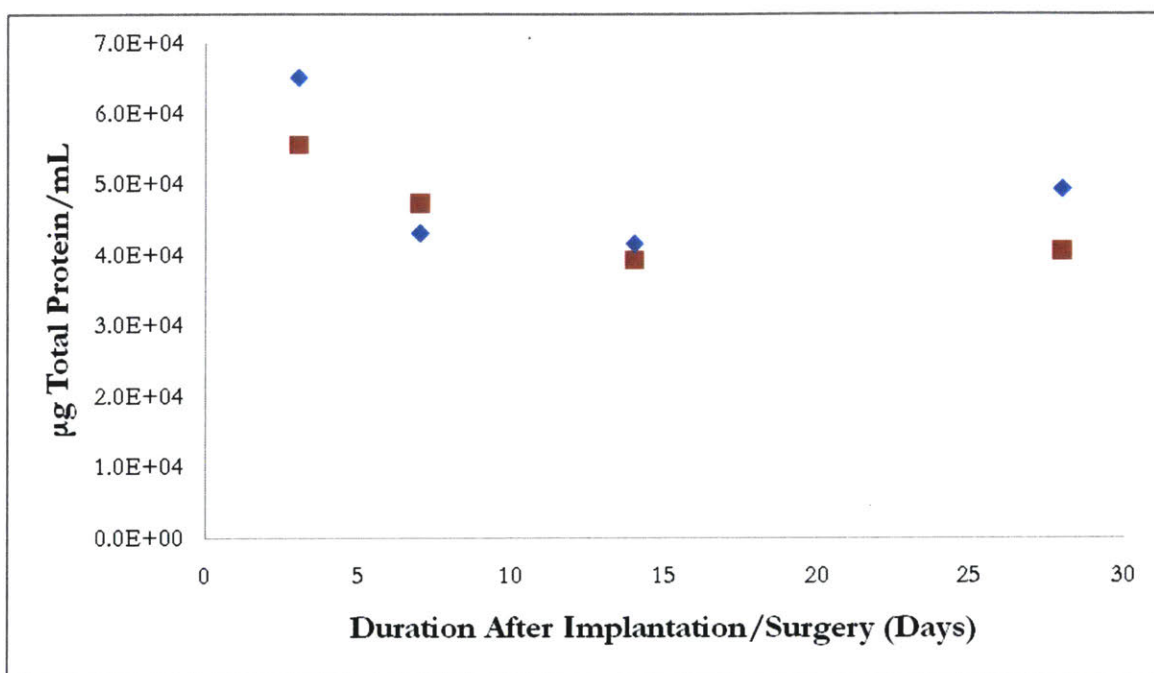
Figure 9. µBCA analysis for total protein concentration 3, 7, 14, and 28 days after implantation (■) and sham (◆) surgeries. Each data point is an average of the total protein obtained from the homogenization and isolation process described in section 2.2.

Shown above, elevated protein levels 3 days post surgery are visible. Observation suggested that levels reached a plateau over the next 25 days. These results lead to the conclusion that both implantation and sham surgeries did elicit an immune response in the rodent brains.

3.3 Immunofluorescence Imaging of GFAP, NeuN, and CD-68

Certain proteins expressed during an immune response in the CNS facilitate new cell development. When new cell growth around the wound is too great, the function of devices in the area can be hampered by biofouling. The relative location and prevalence of GFAP, CD68, and NeuN, all proteins associated with immune response and new cell growth, suggest how and where biofouling may occur. Rodent brains were harvested at each time point post surgery, serially sectioned, and stained with IF conjugated antibodies. Samples were visualized to understand better the extent of the damage and remodeling from implantation and sham surgeries. Under a fluorescent light source, antibodies bound to GFAP and NeuN (stained on separate slices) flouresce green while antibodies bound to CD68 fluoresce red.

Photographs obtained from staining procedures did not exhibit strong fluorescence for any of the assayed proteins. Staining with DAPI did reveal where cell nuclei were relative to one another but did not suggest much in relation to immune response. Figure 10, taken of a brain section harvested 3 days post sham surgery exhibited stronger GFAP/ Anti-GFAP binding than other sections analyzed.
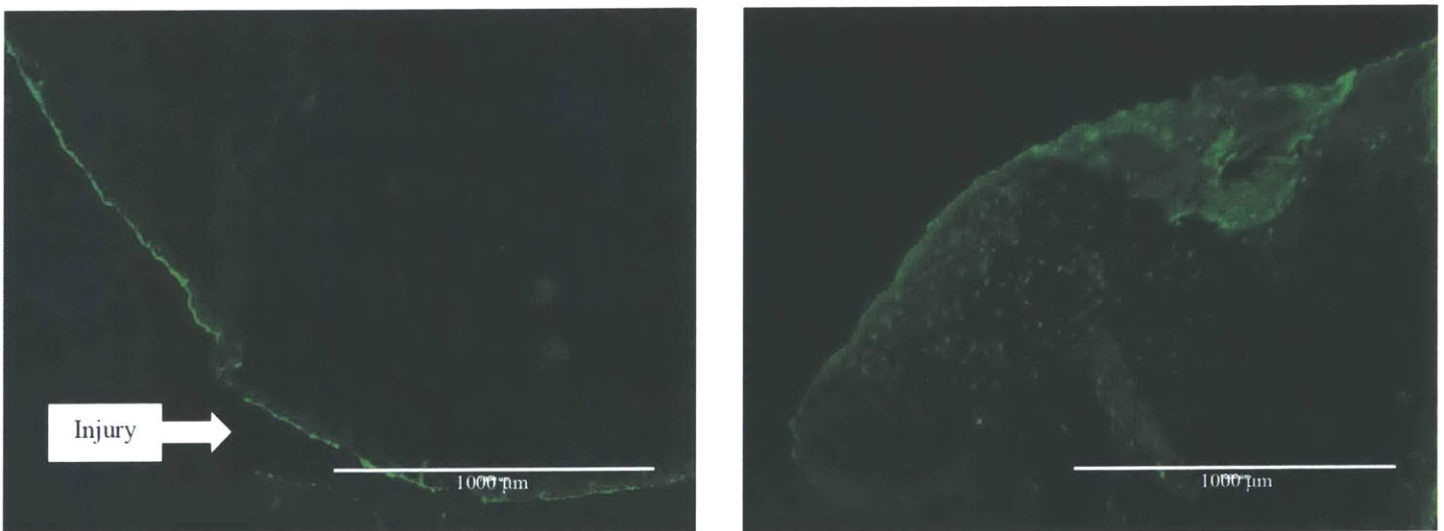
Figure 10. IF image of a 6 μm thick section of rodent brain 3 days post sham surgery. Injured section of the brain (left) and contralateral side (right) of this brain show fluorescence, indicating GFAP expression. Images were taken at 40X magnification on an AMG Evos fl ALL-IN-ONE, digital inverted fluorescence microscope.

Increased levels of GFAP can be seen at the wound site (left) relative to the rest of the brain, but the fluorescence at the injury site does not appear to be greater than that at the uninjured contralateral (right) side. Generally, fluorescence was greater at the edge of the slices, or wherever more surface area was exposed. Overall, staining results were inconclusive and did not show appreciable levels of fluorescence for any of the proteins examined. Closer magnification, as shown in Figure 11, reveals the staining of astrocytes expressing GFAP.

Figure 11. IF image of the contralateral portion of a 6 μm thick section of rodent brain. Section was taken 28 days post sham surgery and stained for GFAP (green) and CD-68 (red). Imaged at 200X magnification on an AMG Evos fl ALL-IN-ONE, digital inverted fluorescence microscope. Boxed portion shows a single astrocytes

Rats undergoing a sham surgery were still expressing GFAP at the wound site 28 days post surgery as illustrated in the figure above. While results obtained from imaging were inconclusive, the above figure does suggest that the cells were expressing GFAP.

3.4 Enzyme Linked Immunosorbent Assay for GFAP concentration

One of the primary markers for new cell growth in the CNS is the presence of Glial

Fibrillary Acidic Protein. Though GFAP's complete function is still unknown, numerous studies

have correlated elevated GFAP levels to astrocyte- mediated wound healing. To ascertain the

extent to which surgery and implantation affect the formation of tissue surrounding a medical

device, a more quantitative measure was needed to determine how GFAP expression changed as

a function of time. The amount of GFAP present relative to total protein in the same sample was

determined at each time point of the study using an ELISA. Standard curves derived from

ELISA analysis yielded an R^2 value > 99%, suggesting an accurate model from which to

ascertain GFAP concentration. Table 3 shows the mean amount of GFAP (ng)/ total protein

concentration (µg) measured in both sham and implant rodents:

Table 3. Average ng GFAP/ µg Total Protein isolated in 0.1g of rat brain 3,7,14, and 28 days post surgery		
	Implanted (ng GFAP/ µg Total Protein)	**Sham (ng GFAP/ µg Total Protein)**
3 Days	0.80	0.81
7 Days	1.85	1.95
14 Days	1.90	1.83
28 Days	2.33	0.79

Note: Final dilution of protein samples used for analysis was 1:12000 and this dilution factor was corrected for in the above table. As previously described, brains were harvested at 3, 7, 14, and 28 days after surgery with "Implanted" referring to surgery in which devices remained in the animal and "Sham" those which the devices were inserted and removed. Data obtained for implanted devices were averaged from a sample size n=4 rodents per duration while n-sham=1.

The lowest concentration of GFAP recorded in brains undergoing both implantation and

sham surgery was seen 3 days post implantation at levels of 0.80 and 0.81 ng GFAP/µg total

proteins, respectively. GFAP concentration in brains that contained the implanted device cap

continued to rise relative to total protein concentration through 28 days post implantation. A

similar trend was seen in brains undergoing a sham surgery until 7 days post surgery. The level

of GFAP peaked at 1.95 ng GFAP/μg total protein, and then declined to initial 3 day levels over the next two time points (0.79 at 28 days vs 0.81 ng GFAP/μg at 3 days). An ANOVA test for significance ($\alpha=0.05$, n=4) was performed on implantation data and revealed no significant difference between concentrations of GFAP (p=0.22>> 0.05). Results from this ANOVA are summarized below in table 4.

Table 4. Analysis of Variance for GFAP, using Adjusted SS for Test						
Source of Variation	SS	df	MS	F	P-value	F crit
Between	3.87	3	1.29	1.74	0.222	3.708265
Within	7.41	10	0.74	-----	-----	-----
Total	11.27	13	-----	-----	-----	-----
S = 0.860562 R-Sq = 34.29% R-Sq(adj) = 14.58% $\alpha=0.05$, n=4* *outliers were removed from 3 Days and 28 Days, yielding n=3						

To examine specific differences between treatment levels, a Tukey Post- Hoc test for between group significance was performed on the data. This analysis did not reveal any hidden significance and specific p-values obtained from the test can be found in table 6 in appendix A. A comparison of the relative increase and decrease of GFAP concentration can be seen more easily in figure 12 below.
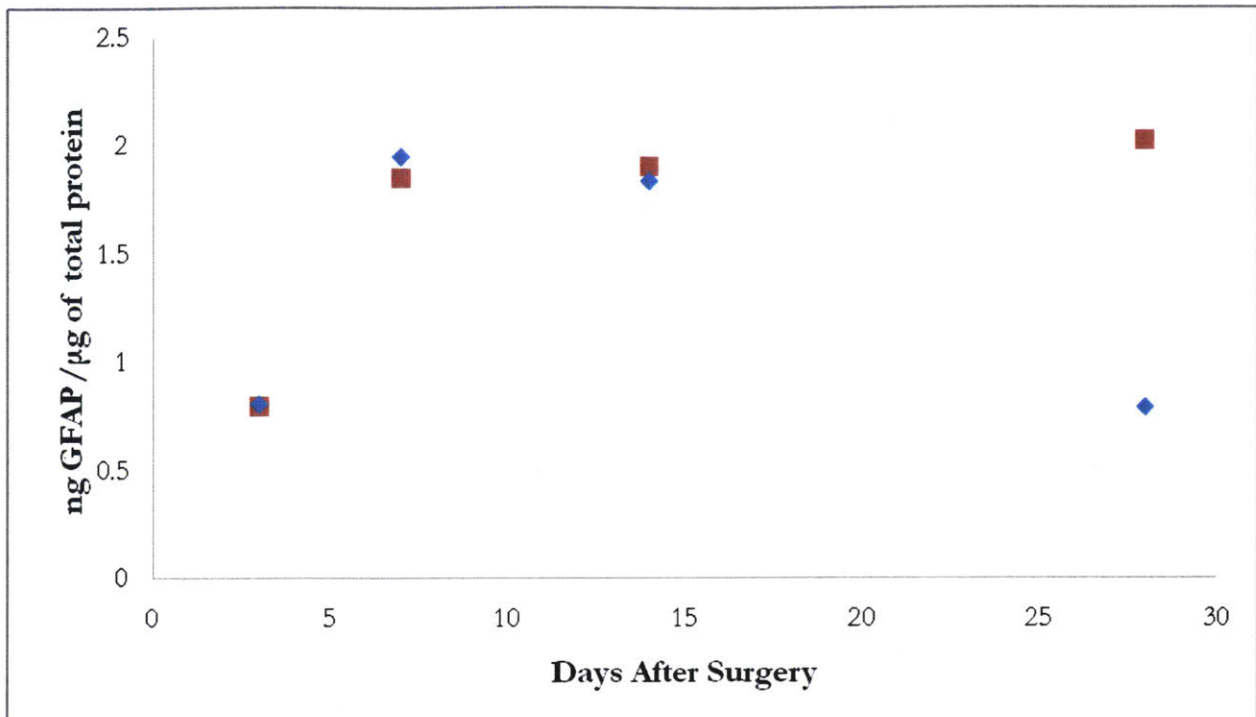
Figure 12. Average GFAP Concentration: Implantation vs. Sham
ELISA analysis for GFAP concentration 3, 7, 14, and 28 days after implantation (■) and sham (◆) surgeries. Each data point is an average of the ng GFAP/ μg total protein recorded for devices from each time point. Results were obtained from the homogenization, isolation, and ELISA methods described in section 2.

GFAP levels for implantation and sham surgeries follow a very similar trend until the 28 day time point. There, a large gap in measured concentration can be observed between the ng GFAP still expressed in brains with devices compared to those without. These data suggest that somewhere between 14 and 28 days, the growth pattern of cells surrounding the injury site changes. It can be surmised that in the absence of any foreign objects, the level of GFAP expressed decreases to initial levels once the wound site has been bridged. When a device is present, the level of GFAP continues to remain elevated as the body strives to build an extracellular matrix around the device [23].

32

4. DISCUSSION AND CONCLUSIONS

This research sought to understand better how introducing a passive diffusion drug delivery device into the brain activates an immune response by utilizing a rodent intracranial implantation model. The implications that a specific immune response holds for biofouling, a phenomenon which can hamper the potency and effectiveness of a drug delivery device, are of particular interest in this research. It is known that upon surgery, the immune response of the CNS is activated, but this research hypothesized that upon the addition of a medical device, the response is prolonged and more aggressive. The incorporation of a foreign body within the brain would prompt the CNS to isolate the impinging device, encapsulating it in tissue and limiting its effectiveness. While histological analysis was inconclusive as to the formation of tissue around implanted devices, analysis of the GFAP ELISA assays suggests that GFAP levels in animals with implanted devices remain elevated compared to levels seen in animals undergoing a sham surgery.

4.1 μBCA Analysis for Total Protein Concentration

Overall, data from μBCA analysis supported the conclusion that the immune response of the brain is activated by surgery. Levels of total protein 3 days post surgery were the highest measured during the experiment. At 55,640 and 65,141 μg/mL of total protein concentration for the implantation and sham, respectively, it can be surmised that inflammation of the affected area occurred. These conclusions are substantiated by ANOVA and Tukey tests which show a statistically significant difference between total protein measured 3 days post implantation and that measured 14 and 28 days post surgery. Additionally, the sharp decline seen in protein

33

concentration of sham samples further corroborates that some response to surgical trauma was initiated.

It should be noted that the sham group saw an increase in total protein concentration from 14 days to 28 days. This increase could be explained by differences in biochemistry and size of rats tested. The import of this particular number should be taken relative to the total amount of a specific protein expression, as is done later with GFAP.

While statistical analysis was possible for the implantation group, the low sample size of the sham group (n=1 per time point) made it impossible to ascribe any weight to statistical analyses performed on this treatment group, or any analyses performed between implantation and sham groups. Comparison on a value by value basis does offer insight to the relative similarities and differences in total protein of both groups. The sharper drop in total protein concentration observed in the Sham group (65,000 to 43,000 µg/ mL from 3 days to 7 days) versus the implantation group (56,000 to 47,000 µg/mL) suggest that inflammatory proteins persisted longer in the implantation groups, though no definitive conclusions can be surmised for this data.

The timeline of decline and subsequent plateau seen in total protein concentration is consistent with that outlined by Stroncek. He writes that in the CNS, inflammation can occur within seconds to hours and persists for hours to days. Once the week timescale is reached, inflammation has nearly subsided and astrocytes begin the process of healing.

Due to monetary and time constraints associated with this work, sample size and duration were limited and placed constraints on possible analysis. To be more conclusive, future assays involving total protein content should be repeated with a larger sample size for both implantation and sham surgeries and should occur over a longer time scale with more data points. This would

34

allow total protein isolated from the implantation and sham rats to be compared statistically and enable researchers to construct a more accurate protein-level graph.

4.2 Immunofluorescence

Histology assays were performed in an effort to visualize better the damage incurred by brain tissue from implantation and sham procedures. Immunofluorescent markers for GFAP, CD68 and NeuN were employed to understand better the specific steps taken by the brain during an immune response, and to determine better where new tissue growth occurs relative to a wound.

Data obtained from this method of analysis were mostly inconclusive and did little to support the original hypothesis of a prolonged immune response in rat brains undergoing implantation surgery. Visualization suggested no difference in concentration of GFAP from one treatment to another and offered little insight into the presence or absence of CD68 or NeuN. Despite the limited fluorescence, it appears that wound sites had a greater concentration of cells expressing GFAP. This phenomenon could be due to a free surface argument as most free surfaces and edges appear to have a greater concentration of GFAP. One hypothesis for this is that the edge provides an increase in surface area for GFAP markers to settle and thus a greater number of the cells expressing the protein are bound.

DAPI staining for cell nuclei was moderately successful and revealed the proximity of astrocytes to one another. Visual inspected suggests that astrocytes may be clustered near wound sites and edges. This result could, again, be attributable to the free surface argument stated above. The complete lack of NeuN and CD68 suggests that staining techniques were inadequate for accurately visualizing these proteins.

Comparisons to literature results reveal a stark contrast. While there are no other studies examining the effect of the same microcapsule device, previous work by Thelin et al. analyzing the effect of other devices on GFAP, CD68, and NeuN expression show increases in expression of the proteins upon injury [26]. The researchers were able to see strong increases in GFAP, NeuN, and CD68 localized to the site of injury.

This histology study was limited by the duration of time under which it was completed. Staining assays were performed once as materials and time constraints limited the means to repeat the assay. The assay could be tailored in the future to better fit the specific requirements of the experiment. Washing solution, primary antibody concentration, incubation time and temperature, secondary antibody concentration, and markers used are all factors which need to be further assessed during further experimentation. Results may have been more conclusive had higher concentrations of GFAP, NeuN, and CD68 been used to facilitate better binding between brain proteins and cell markers.

4.3 GFAP ELISA

An ELISA analysis targeting GFAP quantifies better the immune response elicited by implantation and sham surgeries. Data from the assay show a steady increase in GFAP concentration in the brain, characteristic of new cell growth. The concentration of GFAP rises to an elevated level post surgery as hypothesized, with the rate of GFAP production growing more rapidly a week post initial trauma. Seven days post surgery, brains from the implantation procedure versus those from the sham surgery begin to differ in their GFAP production. Brains harvested from rodents undergoing an implantation surgery continued producing GFAP at an elevated level (increasing mean concentration from 1.90 ng GFAP/ μg total protein to 2.33 ng

GFAP/μg total protein at 28 days post implantation). This is consistent with GFAP levels in brains undergoing a sham surgery, a trend which exhibited a peak concentration at 7 days post implantation and then a subsequent decline to initial levels. Graphical depictions of the data presented in figure 12 illustrate better the similarities between concentrations of GFAP in implantation and sham rodent brains at 3 and 7 days, and to a lesser extent 14 days post surgery. This timeframe corresponds to the point at which the CNS immune response shifts to a new phase. This work suggests that the inclusion of a device prolongs GFAP production.

Even though differences between GFAP levels were not significant, more research is needed to assert this conclusion with greater certainty. Trends in GFAP production in both implantation-treated and sham-treated rodents suggest that the inclusion of an LCP device elicits an immune response which may inhibit the functionality of the device. GFAP has been correlated with the formation of granulomatous tissue and astrocyte production around a foreign body occurs when the body wishes to isolate an object it does not recognize.

Results of this study were consistent with research carried out by Hozumi et al. who reported seeing increases in GFAP mRNA levels in rodents who suffered stab wounds to the brain. His work found elevated levels of GFAP mRNA beginning at day 3 post stabbing and peaking sometime around day 7, eventually returning to pre-injury levels by day 21. The timeline suggested by this work correlates strongly to that seen in the sham surgeries of this research.

One of the limiting factors of this work stems from the low sample sizes studied. Implantation assays had n=4 for each time point. The removal of outliers in the 3 and 28 day post- implantation groups resulted in n=3. Sham results were derived from n=1 as time and budget constraints limited the availability of resources and ability to perform additional

37

surgeries. Future research would benefit greatly from increased sample sizes and more time points, as well as a specific control group of rodents.

Progressing forward, the results of this work are applicable to the design of subsequent iterations of the LCP microcapsule drug delivery device. Devices could be coated with an additional chemical designed to retard the growth of astrocytic cells so biofouling does not become an issue.

Overall, the results of this work suggest that immune responses elicited due to implantation of a device within the brain tissue of a rat are prolonged when compared to a sham surgery. This immune response results in elevated GFAP levels, a protein which may be capable of promoting encapsulation of drug delivery devices and limiting their efficacy. While differences in GFAP levels were not significantly higher after inclusion of a device, the elevated levels may still pose a problem to devices releasing a payload over a long duration. More research is needed to understand better the role an immune response plays in the efficacy of a drug delivery, but a better understanding of the challenges associated with biofouling can lead to preventative measures which increase the effectiveness of treatments.

5 APPENDIX A

Table 5. µBCA Tukey-Post hoc				
	3 days	**7 days**	**14 days**	**28 days**
3 days	-----	-----	-----	-----
7 days	0.108	-----	-----	-----
14 days	0.002	0.0865	-----	-----
28 days	0.004	0.171	0.972	-----
ANOVA result p= 0.002 < α =0.05, n=4				

Table 6. GFAP ELISA Tukey-Post hoc				
	3 days	**7 days**	**14 days**	**28 days**
3 days	-----	-----	-----	-----
7 days	0.4196	-----	-----	-----
14 days	0.3828	0.999	-----	-----
28 days	0.1933	0.883	0.912	-----
ANOVA result: p= 0.222 >> α =0.05, n=4				

RESOURCES

1. American Brain Tumor Association (http://www.abta.org), "Glioblastoma Multiforme (GBM) and Anaplastic Astrocytoma (AA)" Accessed 2010.

2. Anderson JM. Biological responses to materials. Annu Rev Mater Res. 2001;31:81-110.

3. Anderson JM. Inflammatory response to implants. ASAIO Trans. 1988;34(2):101-7.

4. Baker, Sharyn D., Mark Wirth, Paul Statkevich, Pascale Reidenberg, Kevin Alton, Susan E. Sartorius, Margaret Dugan, David Cutler, Vijay Batra, Louise B. Grochow, Ross C. Donehower, and Eric K. Rowinsky: Absorption, metabolism, and excretion of 14C-temozolomide following oral administration to patients with advanced cancer. Clinical Cancer Research 5, 309-317 (1999).

5. Bock, Hans Christoph, et al: First-line treatment of malignant glioma with carmustine implants followed by concomitant radiochemotherapy: a multicenter experience. Neurosurgery Review 33, 441-449 (2010)

6. Conn, P. Michael, ed. *Sourcebook of Models for Biomedical Research*. Totowa, NJ: Humana Press, 2008.

7. El-Kareh, Ardith W. and Timothy W. Secomb: A mathematical model for comparison of bolus injection, continuous infusion, and liposomal delivery of doxorubicin to tumor cells. Neoplasia 2(4), 325-338 (2000).

8. Gelperina, S.E., A.S. Khalansky, I.N. Skidan, et al. Toxicological studies of doxorubicin bound to polysorbate 80-coated poly(butyl cyanoacrylate) nanoparticles in healthy rats and rats with intracranial glioblastoma. Toxicology Letters 126, 131-141 (2002).

9. Gril, Brunilde, Lynda Evans, Diane Palmieri, and Patricia S. Steeg: Translational research in brain metastasis is identifying molecular pathways that may lead to the development of new therapeutic strategies. European Journal of Cancer 46(7), 1204-1210 (2010).

10. Hadjipanayis, Costas G. and Erwin G. Van Meir: Brain cancer propagating cells: biology, genetics and targeted therapies. Trends in Molecular Medicine 15(11), 519-530 (2009).

11. Huang, Qiang, et al: Glioma stem cells are more aggressive in recurrent tumors with malignant progression than in the primary tumor, and both can be maintained long-term *in vitro*. BMC Cancer 8(304), 1-11 (2008).

12. Hozumi, I. Dennis A. Aquino, William T. Norton, GFAP mRNA levels following stab wounds in rat brain, Brain Research, Volume 534, Issues 1–2, 26 November 1990, Pages 291-294, ISSN 0006-8993, 10.1016/0006-8993(90)90142-X. (http://www.sciencedirect.com/science/article/pii/000689939090142X)

13. Mangiola, Annunziato, Pasquale De Bonis, Giulio Maira, Mario Balducci, Gigliola Sica, Gina Lama, Libero Lauriola, and Carmelo Anile: Invasive tumor cells and prognosis in a selected population of patients with glioblastoma multiforme. Cancer 113 (4), 841-846 (2008).

14. Nishikawa, Ryo: Standard therapy for glioblastoma – a review of where we are. Neurologia Medico-Chirurfica 50, 713-719 (2010).

15. Onuki, Y. (2008). A review of the biocompatibility of implantable devices: current challenges to overcome foreign body response. *Journal of Diabetes Science and Technology,* 2(6), 1003-15.

16. Patta, Y. R. Local Exposure and Efficacy of a reservoir-based drug delivery device. Department of Materials Science and Engineering. MIT. (2012)

17. Palmieri, Diane, Daniel Fitzgerald, and S. Martin Shreeve, et al: Analyses of resected human brain metastases of breast cancer reveal the association between up-regulation of hexokinase 2 and poor prognosis. Molecular Cancer Research 7, 1438-1445 (2009).

18. P. Giglio, Chemotherapy for glioblastoma: Past, present, and future," Glioblastoma:, pp. 203-216.

19. Pruthi, Sandhya, M.D. "HER2-positive breast cancer: What is it?" http://www.mayoclinic.com. February 20, 2010.

20. Ratner BD, Bryant SJ. Biomaterials: where we have been and where we are going. Annu Rev Biomed Eng. 2004;6:41-75.

21. Sawyer, Andrew J., Joseph M. Piepmeier, and W. Mark Saltzman: New methods for direct delivery of chemotherapy for treating brain tumors. Yale Journal of Biology and Medicine 79, 141-152 (2006).

22. Scott, Alexander . "Microcapsule Drug Delivery Device for Treatment of Glioblastoma Multiforme."Massachusetts Institute of Technology . (2010): 15-26. Print.

23. Stroncek JD, Reichert WM. Overview of Wound Healing in Different Tissue Types. In: Reichert WM, editor. Indwelling Neural Implants: Strategies for Contending with the In Vivo Environment. Boca Raton (FL): CRC Press; 2008.

24. Stupp, Roger, M.D., et al: Radiotherapy plus concomitant and adjuvant temozolomide for glioblastoma. The New England Journal of Medicine 352(10), 987-996 (2005).

25. The Popular Technology SDS PAGE & Western Blotting :Principle and Application." Web. 22 Mar. 2012.<http://www.toxicology.tcu.edu.tw/files/class_0981/%E7%94%9F%E7%89%A9% E9%86%AB%E5%AD%B8%E6%8A%80%E8%A1%93/980924Gel%20ectrophoresis.p df>.

26. Thelin, J. *et al.* (2011). Implant size and fixation mode strongly influence tissue reactions in the cns. *PLoS One, 6*(1),

27. Thompson JA, Anderson KD, DiPietro JM, Zwiebel JA, Zametta M, Anderson WF, Maciag T. Site-directed neovessel formation *in vivo*. Science. 1988;241(4871):1349-52.\

28. 13 Tse, V. MD, PhD Associate Professor, Department of Neurosurgery, Stanford University Medical Center, Santa Clara Valley Medical Center. Brain Metastasis Medscape Reference

29. Vogelbaum, Michael A.: Convection enhanced delivery for the treatment of malignant gliomas: symposium review. Journal of Neuro-Oncology 73, 57-69 (2005).

30. Voulgaris, S., M. Karamouzis, and N. Papadakis. Intratumoral doxorubicin in patients with malignant brain gliomas. American Journal of Clinical Oncology 25(1), 60-64 (2002).

.31. Yarrow, J. et al. A high-throughput cell migration assay using scratch wound healing, a comparison of image-based readout methods. Journal of BMC Biotechnology. 2004, 4:21

32. Zhou, Rong, Richard Mazurchuk, and Robert M. Straubinger: Antivasculature effects of doxorubicin-containing liposomes in an intracranial rat brain tumor model. Cancer Research 62, 2561-2566 (2002).

33. Ziats NP, Miller KM, Anderson JM. *In vitro* and *in vivo* interactions of cells with biomaterials. Biomaterials. 1988;9(1):5-13.